

Design of the Subsonic Aircraft Roughness Glove Experiment (SARGE)

Michael J. Belisle,¹ Matthew W. Roberts,¹ Matthew W. Tufts,¹ Aaron A. Tucker,² Thomas C. Williams,¹
William S. Saric,³ and Helen L. Reed⁴
Texas A&M University, College Station, Texas, 77843-3141

The Subsonic Aircraft Roughness Glove Experiment (SARGE) is a hybrid natural laminar flow and passive laminar flow control flight test that will be carried out under the auspices of the NASA Environmentally Responsible Aviation initiative. Texas A&M has completed the initial aerodynamic design of a wing glove to be installed on a NASA Gulfstream III testbed. The primary goals of the SARGE experiment are to 1) achieve natural laminar flow to 0.60 chord on the suction side at up to 22 million chord Reynolds number and 2) at conditions of at least 22 million chord Reynolds number, demonstrate the effectiveness of passive Discrete Roughness Elements in extending laminar flow beyond the natural transition location. Computations of the flight test configuration flowfield and the initial design of a laminar flow wing glove are presented, followed by a description of the proposed flight test experiment as well as the instrumentation suite. The initial design is shown to marginally fulfill the design requirements. Efforts are underway to optimize the design to improve spanwise flow uniformity and provide better stabilization of streamwise instabilities.

Nomenclature

| | |
|--------------------------|--|
| AoA_{2D} | = Angle of attack for infinite swept wing, rotated about axis parallel to leading edge |
| AoA_{aircraft} | = Aircraft angle of attack |
| $AoSS_{\text{aircraft}}$ | = Aircraft angle of sideslip |
| c | = Chord length |
| C_l | = Section lift coefficient normalized by local chord |
| C_p | = Pressure coefficient |
| f | = Disturbance frequency (dimensional) |
| H | = Altitude |
| M | = Mach number |
| N | = Smith–Van-Ingén N -factor |
| r | = Leading-edge radius |
| Re_c | = Chord Reynolds number |
| Re_θ | = Attachment-line momentum thickness Reynolds number |
| Re' | = Unit Reynolds number |
| Re_k | = Roughness Reynolds number |
| U_∞ | = Freestream velocity |
| t/c | = Airfoil thickness ratio |
| V_{stall} | = Stall speed |
| x/c | = Chord length ratio |

¹ Graduate Student, Department of Aerospace Engineering, Member AIAA

² Graduate Student, Air Force Institute of Technology Civilian Institution Program, Senior Member AIAA

³ Distinguished Professor, Department of Aerospace Engineering, AIAA Fellow

⁴ Professor, Department of Aerospace Engineering, AIAA Fellow

| | |
|------------------|---|
| $(x/c)_t$ | = Predicted chord length ratio for onset of laminar–turbulent transition |
| α | = Local glove angle of attack |
| α_{\min} | = Minimum test glove angle of attack |
| α_{\max} | = Maximum test glove angle of attack |
| β | = Local glove angle of sideslip |
| ε | = Leading-edge ellipticity |
| A_{LE} | = Leading edge sweep angle |
| λ | = Crossflow wavelength parallel to leading edge (dimensional) |
| λ_{crit} | = Critical crossflow wavelength parallel to leading edge (dimensional) |
| λ_{sub} | = Subcritical crossflow wavelength parallel to leading edge (dimensional) |
| ν | = Freestream viscosity |

I. Introduction

THE Subsonic Aircraft Roughness Glove Experiment (SARGE) is a hybrid natural laminar flow (NLF) and passive laminar flow control (LFC) flight test experiment that will serve as the inaugural research program on the NASA Dryden Flight Research Center (DFRC) Subsonic Research Aircraft Testbed (SCRAT) Gulfstream III aircraft. The project is a part of the NASA Environmentally Responsible Aviation (ERA) program, which has an overall goal of developing technologies to reduce the impact of aviation on the environment. Texas A&M University (TAMU) has designed a flight research program with target conditions of $M = 0.75$ at $H = 30,000\text{--}45,000$ ft, corresponding to a chord Reynolds number, Re_c , between 15–22 million for NLF and 22–30 million for passive LFC. The leading-edge sweep angle, A_{LE} , is approximately 35° . In the NLF range, the glove will demonstrate simultaneous suction- and pressure-side laminar flow.

Saric et al. (1998) discovered that transition delay is possible on a swept wing using a judiciously designed C_p distribution coupled with a passive spanwise-periodic discrete roughness element (DRE) array near the attachment line. The initial Saric experiments were conducted on a swept wing ($A_{LE} = 45^\circ$) in the Klebanoff-Saric Wind Tunnel at $Re_c = 2.4$ million. The Flight Research Laboratory at Texas A&M has completed a successful in-flight demonstration of the use of DREs to passively maintain a laminar boundary layer on a $A_{LE} = 30^\circ$ swept wing at a $Re_c = 8$ million (Carpenter, Saric, & Reed 2010; Saric, Carpenter, & Reed 2011; Rhodes, Reed, Saric, & Carpenter 2010). Roughness receptivity studies are also presently in progress under these conditions in order to quantify the role of roughness amplitude in generating crossflow waves. In addition, this promising technique has been demonstrated for supersonic flight (Saric, Reed, & Banks 2004).

Belisle, Neale, Reed, & Saric (2010) showed that a laminar flow wing glove experiment is feasible at chord Reynolds numbers in the 15–20 million range. The logical extension of these LFC efforts is to extend the technology to conditions relevant to transport-category aircraft: $Re_c = 22\text{--}30$ million with transport-relevant wing lift coefficients. This is the topic of this paper.

Two issues exist related to the application of DREs in LFC. The first is unit Reynolds number, Re' , which governs the roughness Reynolds number, Re_k . The proper sensitivity to roughness must be understood (Rizzetta, Visbal, Reed, & Saric 2010). The second is Re_c , which governs the overall stability behavior. The SWIFT experiments (Carpenter et al. 2010; Saric et al. 2011) were conducted at Re' circa $1.7 \times 10^6/\text{ft}$ which is characteristic of $M = 0.8$ at 40,000 ft. The goal of the present work is to develop an effective flight test to raise the TRL of the DRE technology at Re_c (and Re') characteristic of transports.

II. Experiment concept and testbed overview

SARGE will be the first experiment flown on the NASA SCRAT Gulfstream III research platform (Figure 1). Without SARGE installed, SCRAT has a maximum cruise speed of 0.85 Mach number, a service ceiling of 45,000 ft, and a wingspan of 21.0 m (77 ft 10 in). Following an aircraft search in Belisle et al. (2010), SCRAT represents the most-suitable aircraft for the SARGE flight test program. This was substantiated using a detailed laser scan of the aircraft and corresponding flowfield calculations that show full-aircraft flowfield effects are accountable in the region where the wing glove will be mounted.



Figure 1. View of SCRAT (image courtesy of NASA DFRC)

A. Laser Scanning

Direct Dimensions, Inc. (DDI, Owen Mills, MD) was contracted by DFRC to perform a detailed laser scan and generate a 3D model of SCRAT. DDI used equipment with a single-point accuracy of less than 1 mm from a scanning distance of 15 m. The port side of the aircraft was measured and modeled, treating the vertical plane bisecting the longitudinal axis of the fuselage as a plane of symmetry. DDI fit surfaces to the scanned data point cloud and created the aircraft model.

B. Aircraft Model

The aircraft model generated by DDI was processed further in SolidWorks (Dassault Systèmes, Lowell, MA) to better suit TAMU's CFD needs (hereafter referred to as the TAMU CFD model). The aircraft empennage was removed from the model because it has a negligible influence on the wing, as shown by Rhodes et al. (2008). Neglecting this geometry allowed for a computationally efficient mesh. Results from DFRC, whose CFD models included the empennage, showed good agreement with wing and glove results from TAMU, verifying this approach. The DDI model was quite detailed and prompted the creation of several simplified-geometry models. The primary TAMU CFD model has a simplified engine which removed geometry related to the engine thrust reversers and hush kit. An aircraft model with no engine nacelle and a model of only the aircraft wing were also generated to use in support computations.

C. SARGE Model

The aircraft configuration for the LFC flight tests is an instrumented wing glove (Figure 2). The spanwise extent of the glove is from 42% to 58% semi-span, 1.83 m (72 in) total, located in a region where the engine effects are following from the study in Belisle et al. (2010). The aft extent of the glove is to the rear beam of the aircraft wing on the suction side, roughly $x/c = 0.74$, and to $x/c = 0.37$ on the pressure side. As the pressure side blends into the wing forward of the laminar-flow target, the glove will be designed such that laminar flow is expected to continue onto the existing SCRAT wing surface. The inboard and outboard glove airfoils have chords of 4.83 m (190 in) and 4.01 m (158 in) respectively, with a conical planform that results in $A_{LE} = 34.6^\circ$. This planform layout terminates the glove structure forward of the SCRAT control surfaces (spoilers and flaps). Two spanwise fairings on the inboard and outboard edges of the glove provide smooth transitions from the glove surface to the wing surface, matching geometry, slope, and curvature at the interfaces in order to avoid undesirable disturbance sources. The inboard fairing terminates outboard of the SCRAT wing break and the outboard fairing terminates inboard of the aileron.

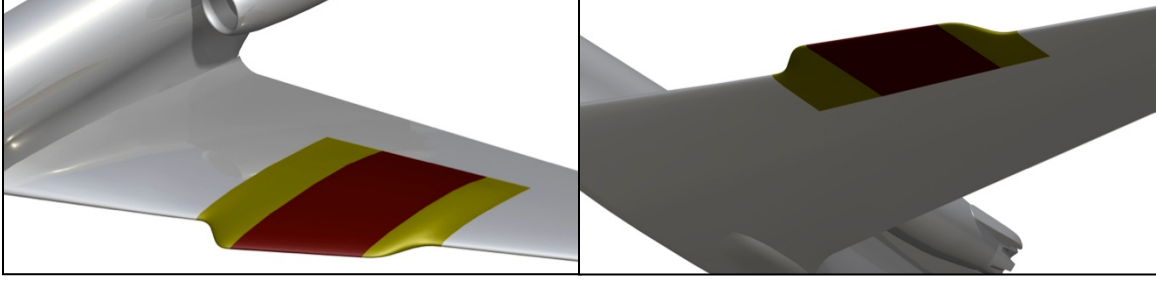


Figure 2. Renderings of wing glove installation on port wing of SCRAT (suction side left, pressure side right)

III. Laminar Flow Control Wing Glove Design and Methodology

We have completed the initial outer mode line (OML) design of a laminar flow wing glove at $M = 0.75$. This design has been analyzed and evaluated in the sections that follow as well as in a companion paper by Malik et al. (2011). The insights gained from these analyses will be incorporated in an optimization routine to refine the design, which will be briefly addressed in Section VI.

The SARGE design must meet a number of requirements as set forth by ERA, which were selected with the goal of realizing an experiment that raises the TRL of DRE technology through flight experiments under transport-relevant conditions. The project requirements can be summarized as follows.

- For $Re_c \geq 15$ million, demonstrate NLF with $(x/c)_{tr} \geq 0.60$ on the suction side over 14 in of span. Demonstrate simultaneous NLF on the pressure side.
- At $Re_c = 22\text{--}30$ million, demonstrate the DRE control that extends laminar flow by at least 50% on the suction side beyond the natural transition location (e.g., if natural transition occurs at $x/c = 0.40$, then DREs will extend transition to $x/c = 0.60$).
- The section lift coefficient requirement for both regimes is $C_l \geq 0.5$ based on the local glove chord within the laminar-flow span. Additional requirements are that $A_{LE} \geq 30^\circ$, $Re' \geq 1.4$ million/ft, and $M \geq 0.72$.
- Since the goal is to demonstrate passive LFC, passive appliqué DREs shall be used, as opposed to other techniques such as plasma actuators or microbubbles. These techniques may be considered in follow-on experiments.
- As crossflow instability is highly sensitive to surface roughness, especially in the leading-edge region, the leading-edge surface roughness shall be varied from approximately $0.3 \mu\text{m rms}$ for a polished leading edge to $4 \mu\text{m}$ for a painted or “operational” leading edge.

A. Design philosophy

Although the philosophies for NLF and DRE LFC design are similar, there are a few important differences that need to be balanced in a hybrid design such as SARGE. The prevailing design philosophy in swept-wing NLF design is to mitigate streamwise and attachment-line instabilities and concentrate on meanflow modifications to reduce the growth of crossflow (CF) waves. This is the focus for SARGE for at least 15 million Re_c up to 20 million Re_c .

In design for laminar flow DRE control, which is the goal here for $Re_c \geq 22$ million, streamwise and attachment line instabilities are also mitigated. In contrast to NLF design, however, there is a focus on *encouraging* crossflow growth in such a manner that shorter wavelengths grow sufficiently and early enough that they may be strategically excited in order to control the most unstable wavelength. The approaches taken towards accounting for these instability mechanisms are as follows.

1. Mitigate streamwise and attachment line instabilities

The initial part of the design procedure is to have an accelerated flow that is subcritical to streamwise instabilities, i.e. Tollmien-Schlichting (TS) waves. When considering natural or passive LFC at flight Reynolds numbers under 50 million, it is not advisable to work at the margins of this instability, and thus this is a goal over the entire SARGE design Re_c range.

The C_p is designed such that the streamwise stability N -factors (log of the amplitude ratio) do not become too large according to the familiar e^N method (for an overview, see for example Arnal and Casalis 2000). Therefore, an

airfoil conducive to LFC by DREs must feature uniformly accelerated flow so that TS waves are controlled where the N -factors remain below $N \approx 7$. With wing sweep, making the pressure gradient more favorable will excite crossflow instability, and therefore a balance must be found between controlling TS and destabilizing CF.

2. Control attachment-line instabilities

Attachment-line instabilities are controlled following a method suggested by Pfenninger (1977) and Poll (1985). The method places a constraint on the leading-edge radius r such that Re_θ , the attachment-line momentum thickness Reynolds number, is less than 100:

$$Re_\theta = 0.404 \sqrt{\frac{U_\infty r \sin^2 \Lambda_{LE}}{(1+\varepsilon)\nu \cos \Lambda_{LE}}} < 100$$

For simplicity, the ellipticity, ε , is taken to be zero (i.e., the worst case).

3. Encourage crossflow growth and allow for DRE control

Stabilizing TS instability naturally encourages crossflow growth. To implement DREs, one recognizes that in the flight environment, stationary crossflow is the dominant instability. One first identifies the most unstable stationary crossflow wavelength, λ_{crit} (it is easiest to reference this length as being parallel to the leading edge). Linear stability theory accurately predicts this critical wavelength and the location at which it first becomes unstable (neutral point). Then one studies stationary crossflow of shorter, *subcritical* wavelengths, λ_{sub} . These are the control wavelengths that the DREs will excite. The observation is that the C_p distribution can be so designed such that these control waves, which are about half the wavelength of the most-unstable wave, will grow sufficiently and then decay subcritically, changing the basic state and preventing the most-unstable wave from dominating. The overall effect is that transition is delayed. The SARGE C_p is designed such that crossflow waves are excited in the DRE regime (again, $Re_c \geq 22$ million) to allow demonstration of DRE control, but stable enough at lower Re_c so that NLF is achieved.

An additional consideration in the crossflow instability is the sensitivity to surface roughness. Unlike streamwise instabilities, which are largely insensitive to surface-roughness, crossflow instability is highly sensitive to roughness. Thus, the quality of finish of the SARGE glove in the leading edge region (approximately $x/c \leq 0.10$) is an important parameter in this experiment. The experiment will consider two surface finishes: a smooth, polished leading edge and a painted or “operational” leading edge similar to a transport aircraft. From Carpenter et al. (2010), the polished surface can sustain crossflow N -factors as high as 14, while the painted leading edge will transition around $N = 9$.

B. Design methodology and workflow

An overview of the iterative design workflow is shown below in Figure 3. The design started with the development of a target C_p assuming an infinite swept wing (block 1). From there, the initial glove geometry was developed by lofting the infinite-swept-wing geometry into a glove and fairing into the SCRAT wing (block 2). In block 3.a, this initial shape was analyzed to determine how well it meets the design requirements. The baseline iteration of blocks 1–3.a. is the state of the design that is presented in this paper.

From here, we obtained insights into what modifications need to be made in the final design. A 3D optimization method (block 3.b) has been developed in collaboration with NASA DFRC. Once this optimization is sufficiently converged, the final design will be verified and refined if necessary by detailed analysis (block 4) that includes fully viscous stability computations and Nonlinear Parabolized Stability Equation analysis to verify the optimized design and quantify the effectiveness of the spacings selected for DRE control. This future work is described briefly in Section VI, although some of these analyses have been carried out on the current design by NASA Langley Research Center (LaRC) and is covered in a companion paper (Malik et al. 2011).

The tasks completed to arrive at the current state of the design will now be described in detail.

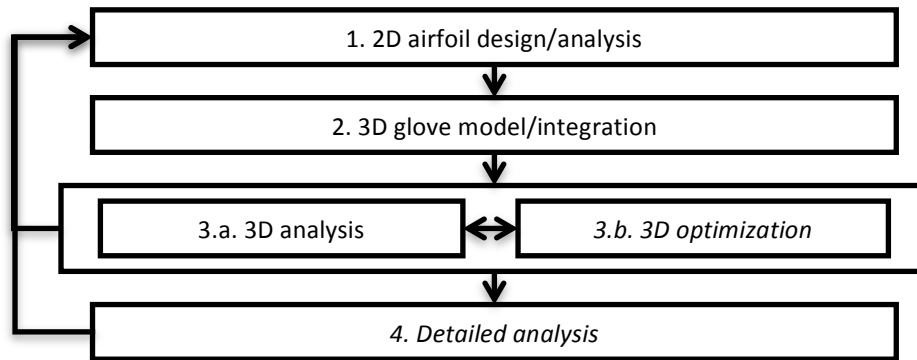


Figure 3. Design iteration workflow

1. 2D airfoil design and analysis methodology (block 1)

The first step in the design process is to design a target C_p distribution by assuming an infinite swept wing. This was achieved through a process that included geometry manipulation using XFOIL (Drela, 1989), inviscid flowfield calculations for an infinite swept wing using GAMBIT and FLUENT (ANSYS Inc., Canonsburg, PA), boundary layer calculations using WINGBL2 (Pruett, 1994), and linear stability theory (LST) calculations using LASTRAC (Chang, 2003), as well as custom scripts and routines to interface results between the codes.

The airfoil cross-section was designed at two span locations, with the airfoil trailing edge fixed to be that of the SCRAT control surfaces (i.e., the G-III wing geometry aft of $x/c = 0.74$ of the G-III wing chord). The mixed-inverse method routine in XFOIL was used to determine the physical geometry from the desired C_p , noting that the trailing-edge portion of the airfoil that is fixed to be the G-III wing geometry. For accuracy in stability calculations, FLUENT was employed to calculate the inviscid C_p used for boundary-layer stability analysis.

LST calculations were performed in LASTRAC using the boundary solution from WINGBL2. The range of unstable frequencies and wavelengths calculated was typically $1 \text{ kHz} \leq f \leq 10 \text{ kHz}$ for a TS wave normal to the leading edge (i.e., zero spanwise wavenumber) and $1 \text{ mm} \leq \lambda \leq 40 \text{ mm}$ for stationary CF ($f = 0$). The WINGBL2/LASTRAC calculations were verified against the Q3BL/LST3D code (Malik 1997) and found to be in good agreement.

2. 3D glove model construction (block 2)

A straight loft between two airfoils located at the inboard and outboard glove boundaries is used to generate the outer mold line (OML) of the wing glove. The curvature-matched spanwise fairings complete the SARGE model. Once the SARGE OML is set, it is outfitted on all clean-wing models previously discussed in Section II.C.

3. Full-aircraft CFD analysis (block 3.a)

With the OML set, the next logical step is to complete full-aircraft computations in order to examine how the flowfield near the glove is affected by effects such as taper, twist, and the pressure field generated by the fuselage and the engine. The C_p used in the infinite-swept wing calculations does not include these effects. These studies allow the listed effects to be accounted for in a manner similar to Rhodes et al. (2008) and Belisle et al. (2010). To study how these differences affect the glove stability characteristics, a grid was generated and full Navier-Stokes computations were performed. Because proper C_p design is critical to stability behavior, the pressure distribution on the glove was examined in detail.

Building on previous experience at TAMU with full-aircraft CFD studies, a flowfield domain was created around the aircraft model. The meshing program ICEMCFD (ANSYS Inc., Canonsburg, PA) was used to generate the grid. A hybrid mesh with both structured and unstructured cells was implemented to accurately and efficiently obtain a solution that captured the flowfield, focusing on adequately resolving the boundary layer on the glove (for future use as described in Section VI.B). Gridding guidelines outlined by the Fourth AIAA Drag Prediction Workshop (Vassberg et al. 2010) served as a reference for generating proper mesh fidelity. The grid can be divided into three primary zones: the freestream zone, the aircraft zone, and the glove zone (Figure 4).

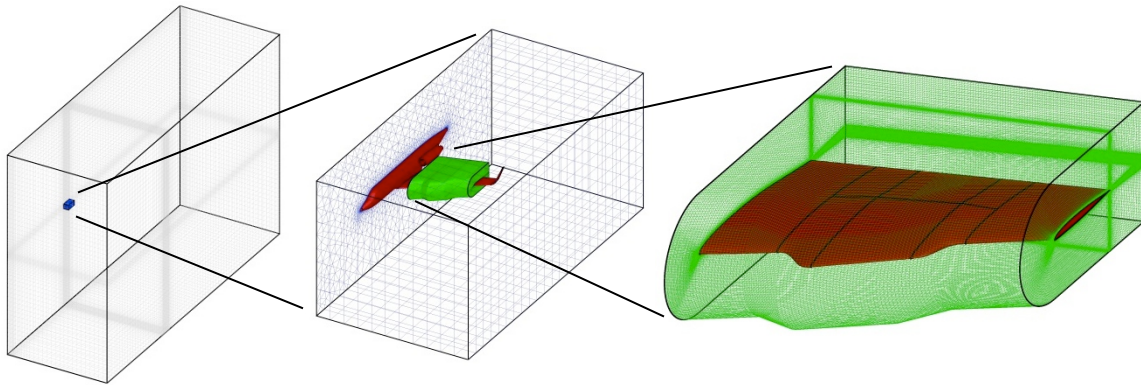


Figure 4. Grid zones (from left to right: freestream zone, aircraft zone, and glove zone)

The freestream zone makes up most of the computational domain and contains structured hexahedral cells, efficiently filling the space.

The aircraft zone surrounds the aircraft and contains unstructured tetrahedral, pyramid, and prismatic cells, which are more suited to meshing the complex shape of the aircraft. Pyramid cells are used to transition between the freestream zone and the aircraft zone, eliminating the need for a grid interface, and prismatic cells are used to capture the flowfield near the surface of the aircraft.

The glove zone is made up of structured hexahedral cells and has a very fine mesh in the boundary-layer region. A grid interface between the aircraft and glove zones was necessary due to disproportionate cell size and shape. Simulation results showed that flowfield discontinuities at the interface were minimal and would not adversely affect the solution.

During the initial full-aircraft CFD simulations, it was discovered that converged laminar solutions would not be possible due to flow separation. Turbulence models would need to be employed, but a fully turbulent boundary layer would produce inaccurate laminar boundary-layer stability calculations. The glove zone was subsequently split into laminar and turbulent subzones. Turbulence quantities are still transported in the laminar subzone, but turbulence production is disabled. The laminar subzone extends completely across the glove spanwise and back to the pressure minimum, where the flow separation begins (Figure 5).

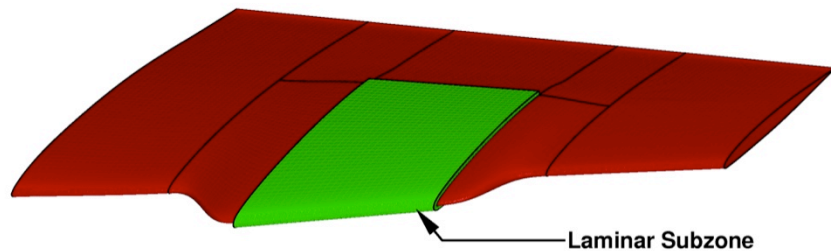


Figure 5. Rendering of laminar subzone location and extent

In order to check grid independence, several approaches were employed or are in progress. First, flowfield results from simulations using different grids generated at TAMU were compared, with variations in the design, level of refinement, and flowfield domain size. The agreement between solutions from all grids was quite good. Second, results from TAMU simulations were compared to results from DFRC and LaRC, which used different CFD codes and grids. Result agreement between the different organizations was also quite good. Third, the boundary-layer stability calculations performed on TAMU simulation results using various grids will be compared. Because the current glove will not be used as the final SARGE design, a detailed comparison of stability results was not completed but is planned for the refined design iterations.

All full-aircraft CFD studies completed by TAMU were solved with FLUENT. A viscous, density-based solver was used and compressibility effects were included. The $k-\omega$ shear-stress transport model developed by Menter

(1993) was implemented with turbulence disabled in the laminar subzone to simulate laminar flow on the glove. The primary full-aircraft computational test point has the following conditions: freestream velocity of 0.75 Mach number, free-stream static pressure of 19.9 kPa abs (2.90 psia), and a static temperature of -56.5°C (-69.7°F). The atmospheric values used are specified by the US Standard Atmosphere 1976 for an altitude of 38,840 ft, resulting in mid-span glove $Re_c = 22$ million. Air density and viscosity are calculated with the ideal gas model and Sutherland's law respectively. The aircraft angle of attack is $AoA_{\text{aircraft}} = 3.5^\circ$, iteratively chosen to generate the desired C_p at the mid-glove streamwise airfoil, and the aircraft angle of sideslip is $AoSS_{\text{aircraft}} = 0.0^\circ$.

A pressure far field was applied to the far-field surfaces of the computational domain, employing the conditions listed above. Because only half of the model has been included up to this point, a symmetry boundary condition was applied to all surfaces coplanar with the aircraft symmetry plane. Aircraft surfaces were modeled as no-slip walls, with the exception of the engine intake and exhaust. The engine intake was modeled as a pressure-outlet with a specified mass flow rate and the engine exhaust was modeled as a pressure-inlet. A 1D engine model developed by DFRC provided the engine boundary conditions based on the far-field conditions.

IV. Intermediate design results and discussion

A. Infinite swept wing

Two airfoil sections, designated as TAMU2D-04-BL198 at the inboard extent of the glove and TAMU2D-04-BL270 outboard, nominally achieve the design requirements. The glove has a taper ratio of 0.83. The resulting design meets the primary NLF targets on the suction side and pressure sides. Possibilities for DRE control are also established, but some modifications to the C_p are necessary to properly demonstrate DRE LFC over a range of conditions. Summary parameters of the designed airfoil are shown in Table 1.

Table 1. Airfoil section design summary.

| | TAMU2D-04-BL198 | TAMU2D-04-BL270 |
|------------------------------------|--------------------------------|--------------------------------|
| M (primary design) | 0.75 | 0.75 |
| Re_c (primary design) | 22.0×10^6 | 22.0×10^6 |
| c (m, streamwise) | 4.8 m (16 ft) | 4.0 m (13 ft) |
| H (ft) | 40,700 | 36,800 |
| t/c (streamwise) | 10.0% | 10.7% |
| r | 18 mm @ $AoA_{2D} = 2.6^\circ$ | 16 mm @ $AoA_{2D} = 2.7^\circ$ |
| Re_θ ($Re_c = 30$ million) | 85 | 87 |
| C_l | 0.50 @ $AoA_{2D} = 2.2^\circ$ | 0.50 @ $AoA_{2D} = 2.4^\circ$ |

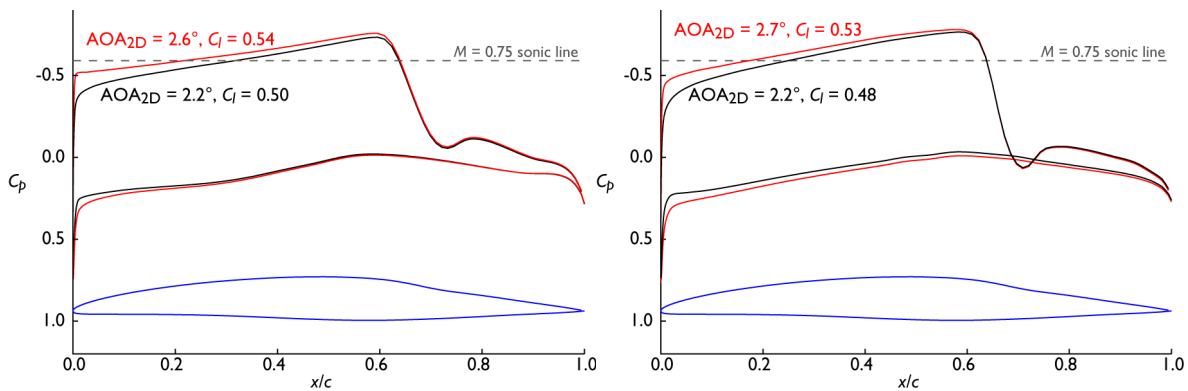


Figure 6. TAMU2D-04-BL198 (left) and TAMU2D-04-BL270 (right) infinite-swept-wing C_p curves.

As shown by the pressure distributions in Figure 6, TAMU2D-04-BL198 achieves the target $C_l = 0.5$ at $AoA_{2D} = 2.2^\circ$, where AoA_{2D} is the airfoil angle-of-attack when rotated about an axis parallel to the leading edge. The

maximum angle-of-attack for this airfoil is $AoA_{2D} = 2.6^\circ$ with $C_l = 0.54$, thereafter an early suction peak is developed on the suction side that is expected to cause early transition due to TS breakdown. The suction peak is at $x/c = 0.60$ on the suction side and $x/c = 0.55$ on the pressure side.

For TAMU2D-04-BL270, $C_l = 0.5$ is obtained at $AoA_{2D} = 2.3^\circ$, while the maximum $AoA_{2D} = 2.7^\circ$ and $C_l = 0.53$. The pressure minima are at approximately $x/c = 0.60$ on the suction side and $x/c = 0.55$ on the pressure side.

Both airfoils develop supercritical flow, achieving maximum $M \approx 1.2$ at $x/c \approx 0.6$. Although the transition to 3D waves as the Mach number exceeds unity is a particular concern for streamwise instability, crossflow instability is relatively insensitive to compressibility effects (Arnal and Vermeersch, 2011). Detailed analysis on the final C_p will include consideration of 3D streamwise instability waves.

Linear stability calculations using LASTRAC verify that the airfoil C_p distributions minimize TS instabilities for waves in the direction normal to the leading edge, while permitting only modest growth of stationary CF waves. The N -factors at $AoA_{2D} = 2.2^\circ$ are shown in Figure 7. Transition estimates are summarized in Table 2. Only TAMU2D-04-BL198 results will be discussed and presented in detail; results at the outboard section are qualitatively similar.

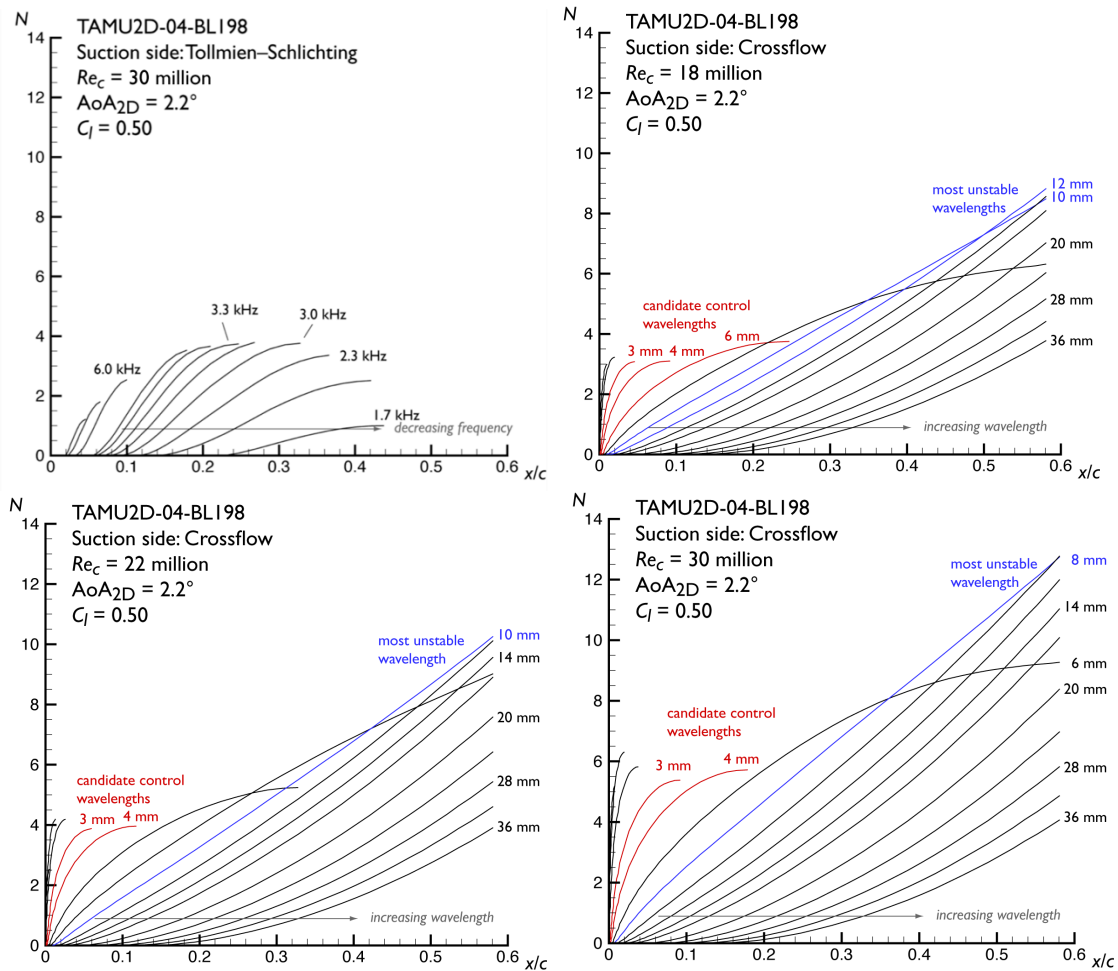


Figure 7. LST N -factor results at $AoA_{2D} = 2.2^\circ$ on the suction side of TAMU2D-04-BL198. $Re_c = 18$ million corresponds to NLF conditions, while $Re_c = 22$ million and 30 million correspond to DRE LFC conditions.

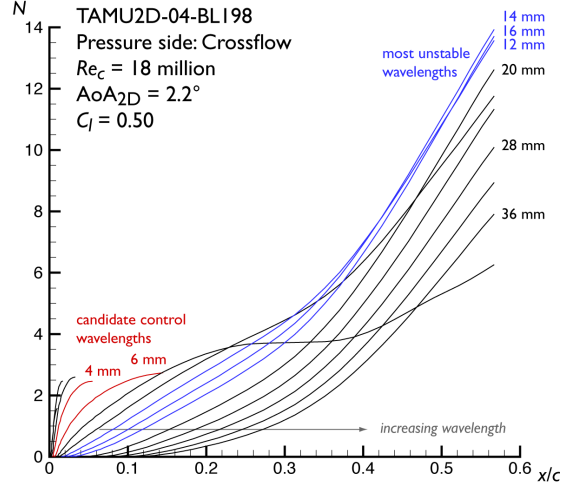


Figure 8. LST N-factor results at $AoA_{2D} = 2.2^\circ$ on the pressure side of TAMU2D-04-BL198 for NLF $Re_c = 18$ million condition.

At $Re_c = 18$ million, NLF is achieved to approximately the target x/c for both polished ($N=14$) and painted ($N=9$) surface finishes, as the most unstable wavelength $\lambda = 12$ mm reaches a maximum value of $N = 8.3$. For the pressure side shown in Figure 8, the most unstable waves of $\lambda = 12-16$ mm reach $N = 9$ at $x/c = 0.45$ and maximum value $N = 13.5$ at $x/c = 0.57$. Thus, the SARGE glove should be able to demonstrate simultaneous suction- and pressure-side NLF.

At $Re_c = 22$ million, the most unstable wavelength is $\lambda = 10$ mm, which reaches $N = 9$ at $x/c = 0.52$, and a maximum $N = 10$ at $x/c = 0.58$. Candidate control wavelengths are in the range $\lambda = 3-5$ mm. At $Re_c = 30$ million, the most unstable wavelength is now $\lambda = 8$ mm, with the control wavelengths again in the $\lambda = 3-5$ mm range. The $\lambda = 8$ mm wave reaches $N = 9$ at $x/c = 0.40$.

Concluding from these results, it appears that this airfoil could serve as an NLF design all the way up to $Re_c = 30$ million for a polished leading edge. For DRE control with a painted finish, it is necessary to operate at $Re_c = 30$ million (where transition is expected to occur at $x/c = 0.40$) in order to be able to demonstrate a 50% laminar-flow increase before reaching the suction peak at $x/c = 0.60$. For these reasons, in addition to some concerns identified by Malik et al. (2011) for streamwise instability waves in directions other than perpendicular to the leading edge, the C_p will be refined in the final design to further destabilize crossflow and alleviate concerns about streamwise instabilities.

Table 2. Summary of suction-side crossflow transition locations for TAMU2D-04-BL198. $N=14$ is assumed for a leading edge with a polished finish, $N=9$ for an painted leading edge finish.

| AoA_{2D} | Re_c | C_l | $(x/c)_{tr}$ ($N=14$) | $(x/c)_{tr}$ ($N=9$) |
|-------------|--------|-------|----------------------------|---------------------------|
| 2.2° | 18 | 0.50 | ≥ 0.58 | ≥ 0.58 |
| 2.2° | 22 | 0.50 | ≥ 0.58 | 0.52 |
| 2.2° | 30 | 0.50 | ≥ 0.58 | 0.40 |
| 2.6° | 18 | 0.54 | ≥ 0.58 | ≥ 0.58 |
| 2.6° | 22 | 0.54 | ≥ 0.58 | ≥ 0.58 |
| 2.6° | 30 | 0.54 | ≥ 0.58 | ≥ 0.58 |

B. Full-aircraft computations

1. Glove Pressure Distribution

The pressure distribution on the glove surface was examined in order to determine stability characteristics at different semi-span locations. Upon the completion of full-aircraft simulations on this initial glove model, several differences between the 2D infinite-swept-wing computations and full-aircraft computations were identified.

The first difference is visible in the C_p distribution. Figure 9 shows a comparison of the infinite-swept-wing C_p (calculated assuming an infinite-swept-wing for a slice of the lofted glove geometry at the mid-span location) and the full-aircraft C_p at the mid-glove-span location. There is reasonable agreement near the leading edge, but a much steeper pressure gradient in the full-aircraft computations aft of $x/c = 0.35$. In addition, there is a shock on the suction side of the glove that was not present in any 2D calculations. Due to its mild nature and location aft of the test surface, the shock is not a major concern.

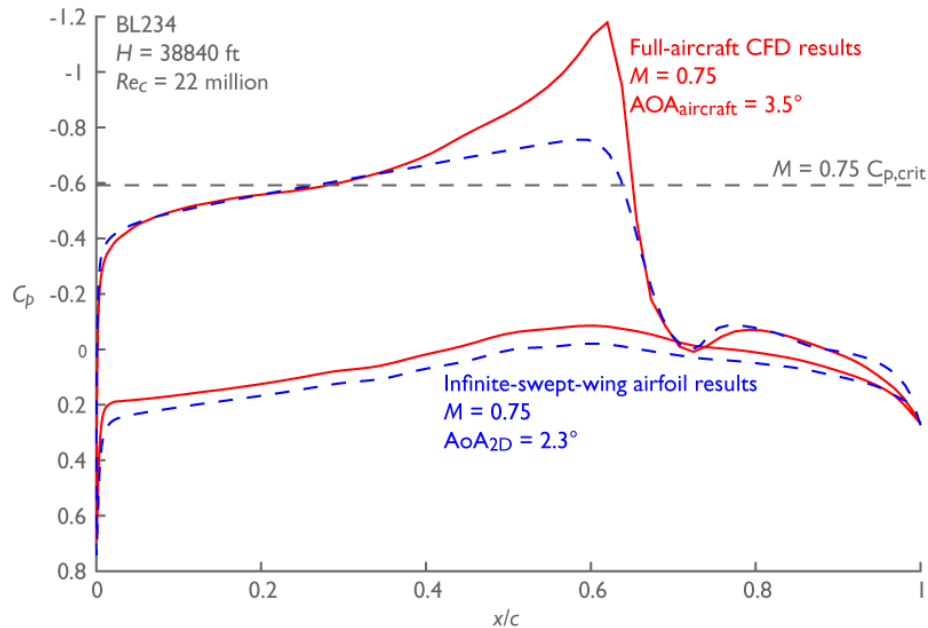


Figure 9. Comparison of infinite-swept-wing airfoil C_p (dashed line) and full-aircraft glove C_p (solid) at mid-span glove location.

The second was an AoA mismatch between 2D and full-aircraft simulations based on pressure distributions generated by each simulation. Knowledge of this behavior is useful since AoA is a critical parameter that must be planned for not only during the design stages but during flight testing as well. For this reason, a procedure for determining the AoA data band in flight is described in Section V.B.

The third and most significant difference was substantial spanwise variations in the pressure distribution on the suction side of the glove. Figure 10 displays C_p contours on the glove, the glove fairings, and a portion of the wing. The iso-lines crossing the glove do not maintain a constant relative x/c position, indicating that the current glove design is not generating a spanwise uniform pressure distribution. Figure 11 shows the extent of the variations with sectional C_p distributions at various buttock lines across the glove, ranging from the inboard edge to the outboard edge in 0.15 m (6.0 in) increments. Even with this spanwise variation, however, inspection of the C_p curves suggests an approximately 30-in wide span of reasonably uniform flow, which is more than sufficient to meet the 14-in laminar-flow span requirement.

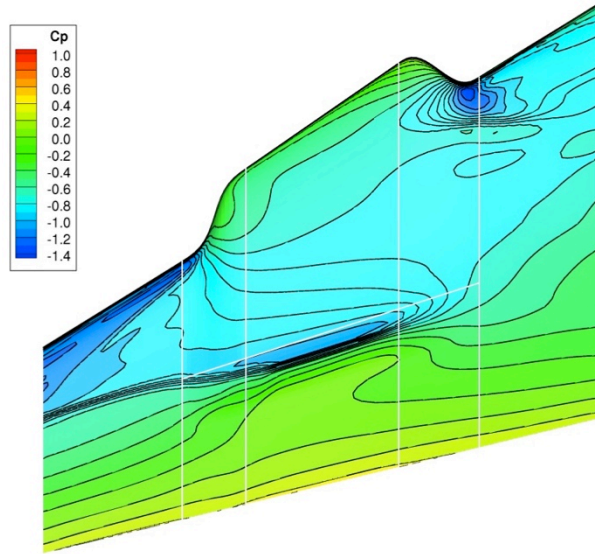


Figure 10. Pressure coefficient contours on the suction side of the wing, glove, and glove fairings.

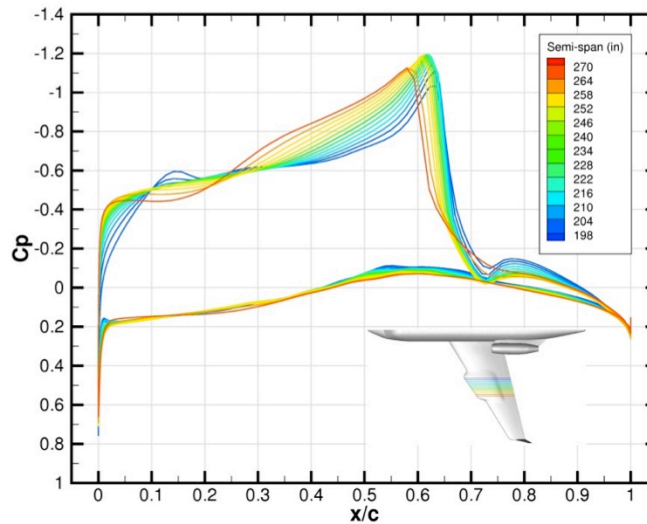


Figure 11. Pressure coefficient distributions at various span locations across the glove

An effort to generate an optimized glove OML with improved spanwise-uniform flow and better C_p matching (that accounts for the various 3D effects not present in the infinite-swept-wing analysis) is covered in Section VI.A. The OML presented here is used to initialize the C_p -matching routine.

2. Full-aircraft glove mid-span section stability results

On account of the spanwise non-uniformity, the results presented here will focus on the mid-span C_p . LST stability calculations on this section are presented in Figure 12 and the pressure-side in Figure 13. The N -factors for TS waves normal to the leading edge are encouraging, as the factors are largely unchanged from the infinite-swept-wing results presented in Figure 7. Crossflow results show that $Re_c = 17.5$ million will achieve NLF to $x/c = 0.60$ for a polished leading edge, and transition is expected to occur at $x/c = 0.45$ for a painted operational leading edge. On the pressure side, transition is expected at $x/c = 0.58$ for polished leading edge and $x/c = 0.41$ for painted.

At the start of the DRE LFC range, $Re_c = 22$ million, natural transition due to the $\lambda = 10$ mm disturbance is expected at $x/c = 0.58$ (polished) and $x/c = 0.41$ (painted). Thus, for this design, the painted leading edge is required in order to demonstrate the DRE control requirement of 50% transition delay. In this case, $\lambda = 3-4$ mm is the candidate control wavelength range.

At $Re_c = 27.5$ million N -factors for the control wavelengths are higher than desired, as the shorter wavelength $\lambda = 3$ mm reaches $N = 6.1$, which doesn't allow sufficient margin for excitation before reaching an N -factor where the DREs themselves would cause early transition. Natural transition is expected to occur at $x/c = 0.50$ (polished) and $x/c = 0.38$ (painted). Thus, a principal goal in the optimization is to reduce the growth of the smaller wavelengths so that control can be demonstrated over a broader C_p range.

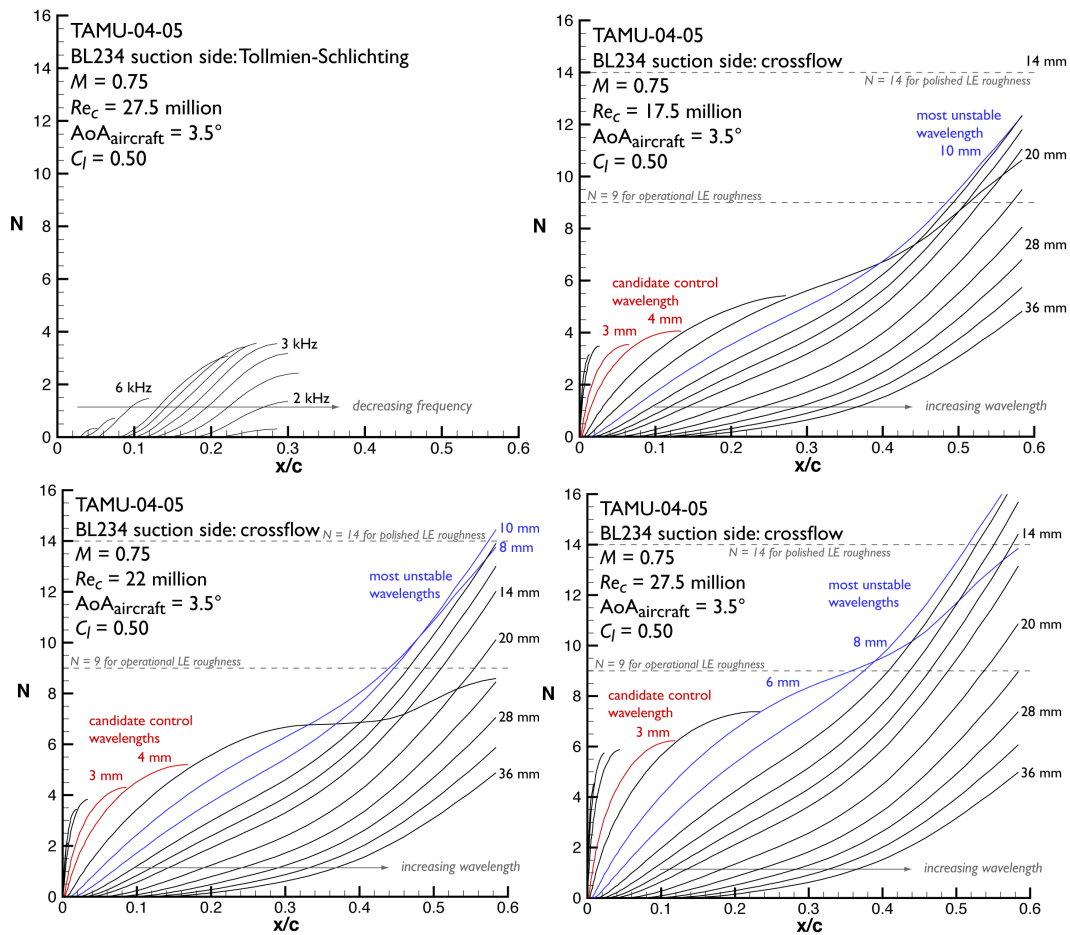


Figure 12. BL234 suction-side LST stability results, $AoA_{aircraft} = 3.5^\circ$. From top left: TS normal to leading edge; crossflow at $Re_c = 17.5$ million (NLF), $Re_c = 22$ million (DRE), and $Re_c = 27.5$ million (DRE).

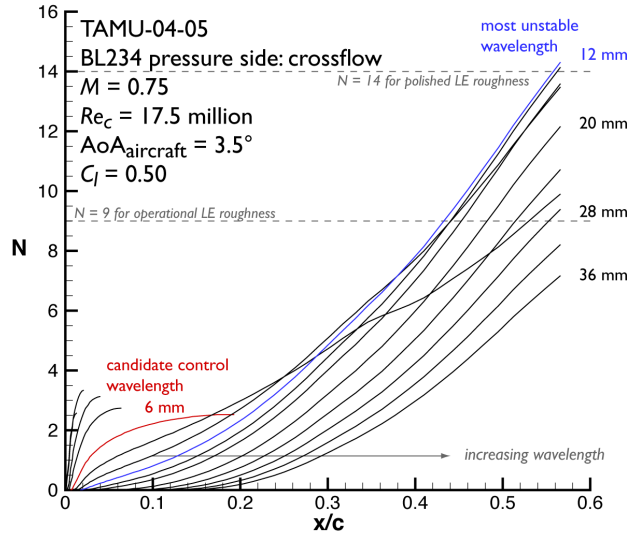


Figure 13. BL234 pressure-side LST stability results, $AoA_{aircraft} = 3.5^\circ$. Crossflow at $Re_c = 17.5$ million (NLF).

V. Flight experiment

The flight experiment has been designed to demonstrate NLF and LFC control using spanwise-periodic DREs at transport-relevant flight conditions (Figure 14). The flight experiment requires the computational models previously described in order to safely and efficiently gather a complete data set. Next, a flight test technique was designed. A test plan was developed with a building-block approach to efficiently gather and analyze the flight data. Finally, the instrumentation suite will be discussed. The safety plan is under development in concert with NASA DFRC and is beyond the scope of this paper.

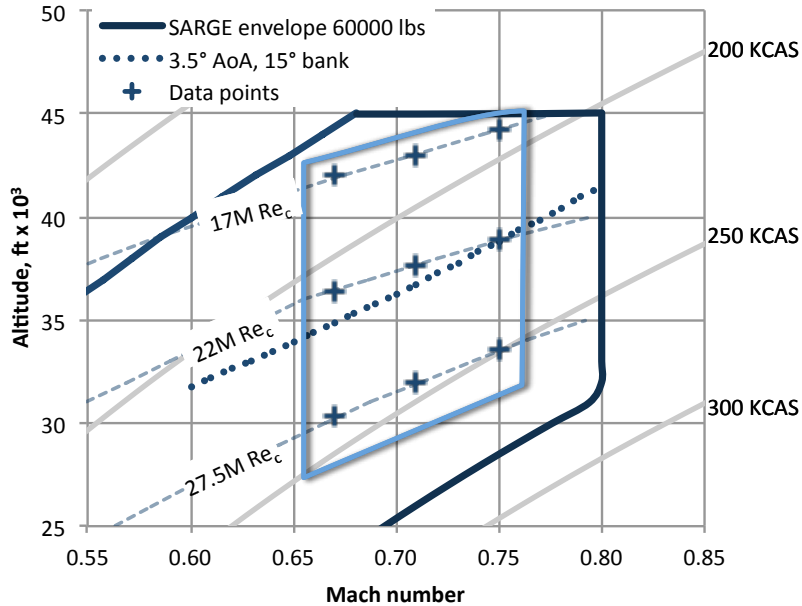


Figure 14. SARGE flight envelope with inscribed science envelope

A notional science envelope is inscribed within the SARGE flight envelope (Figure 14). Constant-Reynolds number isobars are depicted using the reference length of the mid-span SARGE glove chord. As the SARGE glove is tapered, the inboard section will experience higher Re_c while the outboard section will experience lower Re_c . Thus, the science envelope illustrates the capability of SARGE to achieve transport-relevant flight conditions on the glove test section: 0.75 Mach number and 15–30 million Re_c . Test objectives require demonstration of NLF at flight conditions greater than 15 million Re_c and demonstration of DRE effectiveness at flight conditions greater than 22 million Re_c . A Re_c greater than 30 million is beyond the scope of the current investigation. Current models show supercritical flow on the SARGE glove test section at 0.75 Mach number, so the science envelope extends to lower Mach numbers where the glove test section should be fully subcritical (< 0.70 Mach number). This flexibility anticipates the possibility that supercritical flow may affect the SARGE NLF characteristics and DRE effectiveness and will allow the SARGE glove to gather important flight data at subcritical transport-relevant flight conditions.

A. Flight Test Technique

The SARGE glove is designed to demonstrate NLF and DRE effectiveness within a narrow angle-of-attack range. Therefore, a stabilized flight condition is critical to the analysis and validation of computational models. These factors require a stabilized flight maneuver which enables very precise control of angle of attack, sideslip, and Mach number. The flight test technique was designed around a constant speed, constant altitude, low-bank-angle turn in visual flight conditions (clear of clouds) with smooth air. Speed will be controlled with throttle adjustments. An altitude will be selected to provide the target Reynolds number and controlled with pitch inputs (probably autopilot). Rudder inputs will be used to control the angle of sideslip resulting in an effective angle of wing sweep on the SARGE glove. Up to 30° of bank will be selected to vary load factor which will provide fine control over the aircraft’s effective gross weight (subject to safety of flight analysis). This combination of speed, altitude, and effective gross weight will effect the target angle of attack on the SARGE glove. In order to increase test efficiency, a model was created which calculates the flight condition (i.e., Mach number, altitude, gross weight, bank angle) corresponding to a desired angle of attack (e.g., Figure 14 dotted line). This model will be invaluable for visualizing operations within the science envelope, planning research sorties, and producing bank angle estimates for the pilot during execution. As flight data are collected, the model can be refined to accurately predict SCRAT performance with the SARGE glove installed.

Fine control of the flight conditions will be very challenging but practicable through balancing the concepts of data band and tolerance. A data band is defined as the range within which the datum point is valid. The tolerance is how much a valid datum point can vary. In this experiment, the parameter data bands are relatively large, which makes a stabilized flight conditions easy to execute. The tolerances, however, are tight and a challenge to hold. This balance allows the pilot to concentrate on holding four parameters to tight tolerances about a flight condition within a comfortable data band (Table 3) for 15 continuous seconds. The task of holding tight tolerances on multiple exact, predetermined parameter values is not practicable and would result in an inefficient flight test experiment.

Table 3. Flight parameter data bands and tolerances

| | Data band | Tolerance |
|-------------------|--|---------------------|
| Mach number | subcritical [0.66, 0.70] [*] supercritical [0.70, 0.76] [*] | ± 0.01 |
| Reynolds number | NLF [15, 30] $\times 10^6$ DRE [22, 30] $\times 10^6$ | $\pm 2 \times 10^5$ |
| Angle of attack | $[\alpha_{\min}, \alpha_{\max}]^{**\dagger}$ | $\pm 0.1^\circ$ |
| Angle of sideslip | $[-1^\circ, +1^\circ]$ | $\pm 0.1^\circ$ |

^{*}Specific values to be determined during science envelope definition block.

[†]The magnitude of the range is expected to be approximately 0.5° .

In general, the management of four simultaneous flight parameters to tight tolerances would be a very challenging task. However, this challenge is mitigated by the judicious application of data bands coupled with a suite of precision instruments. While the research team needs precise knowledge of flight conditions in order to validate numerical models, the specific value can be captured within a data band. The Mach numbers of interest are divided into two data bands: supercritical has sonic flow on the SARGE glove and subcritical is fully subsonic. The specific values are based on numerical calculations which will be validated with flight data. Mach numbers in the

supercritical data band are relevant to transport category aircraft which are the subject of the current investigation. The Reynolds number data bands are based on test objectives designed to provide transport-relevant flight conditions, and the reference length is the mid-span chord length of the SARGE glove. The angle of attack data band is referenced to the pressure coefficient distribution of the SARGE glove and shall produce transport-relevant lift coefficients ($C_l \geq 0.5$). The angle of sideslip affects the effective sweep angle, and the data band was selected to maintain a nominal wing sweep similar to the Gulfstream III host aircraft.

Another technique employed to mitigate the challenge of holding four simultaneous flight parameters to tight tolerances is a dedicated flight display for the research pilot. This display provides only the data that the pilot needs in an intuitive format with very little time delay. The four parameters (Mach number, Reynolds number, angle of attack, and angle of sideslip) and their tolerances (Table 3) are presented with analog slide bars to present trend and rate information to the pilot (e.g., Figure 15). The slide bars are aligned such that the target values create a horizontal line in the middle of the display. The flight parameter tolerance is set as the first tic mark on the bar and constitutes the majority of the space on the slide bar. This region and is dedicated to displaying trend and rate information to the pilot since these are the ranges which must be most carefully controlled. The next region of the slide bars represent the data band where the data are relevant. Finally, the limits of the slide bar scales are set to operationally relevant flight conditions so that the moving pointer doesn't go off scale (and therefore, unusable) during transitions from test point to test point.

While the SCRAT testbed has production flight instruments, the flight conditions of interest to the research as located at the SARGE glove on the port wing (Figure 2). The glove angle of attack (α) is positioned at the outboard side of the display since it is associated with the pitch axis and primarily controlled with the pilot's yoke hand. Similarly, Reynolds (Re_c) and Mach numbers (M) are positioned on the inboard side of the display next to the throttles. The glove angle of sideslip (β) scale is aligned horizontally since it is a lateral axis and primarily controlled with rudder.

These flight conditions need to be precisely measured by an instrumentation suite (section V.C) and presented to the pilot with very little time lag. Typically, aircraft handling qualities with a time lag greater than 100 ms between control input and pilot feedback invites pilot-induced oscillation (PIO) (MIL-F-8785C, 1980). This necessitates a dedicated display which runs independently of a desktop operating system. Electronic displays can be configured according to the task requirements and can leverage advanced features to communicate information to the pilot. For example, the indices can be configured for a specific flight condition, markers can change colors according to their position or rate, and pilots can arrange the information according to personal preference. For example, Figure 15 reflects the 22 million Re_c , 0.75 Mach number data point shown in Figure 14.

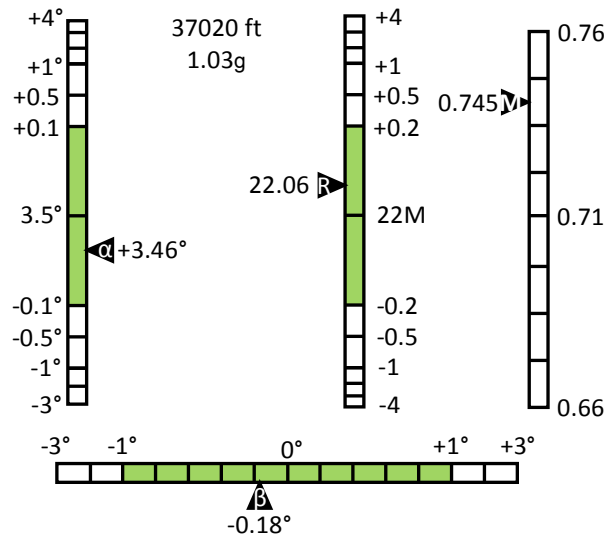


Figure 15. Notional research pilot flight display

B. Test Plan

The test plan describes three blocks which each develop understanding of the flight characteristics of SCRAT with the SARGE glove installed then instructs the specific flight conditions to be used in subsequent blocks. The approach requires precise control of flight conditions that can be repeated across sorties as described by the flight test technique. Careful design of the instrumentation package and analysis plan and an experienced research flight crew are critical to successful acquisition of data. Sorties dedicated to clearing the flight envelope of the SARGE glove and instrumentation structures will precede sorties where data are collected. Overall, the scope of the flight experiment includes 36 to 47 data sorties totaling 74 to 97 flight hours. The initial sorties will refine the science envelope from prediction to actual operations and determine the angle of attack data band and target value for the remainder of the experiment. NLF sorties will determine the effect of Reynolds number on the location of transition and set the baseline flow characteristics. DRE sorties will determine the effects of DREs on the transition point for a selection of DRE configurations.

Science envelope definition sorties are the initial data flights and will refine the science envelope using flight data rather than predictions. This block is expected to consume 2 to 3 sorties and 6 to 9 flight hours. First, the research air data system will be calibrated within the science envelope using either a differential GPS or calibrated pacer aircraft truth source. Next, the SARGE glove will be configured with a leading edge equipped with static pressure ports. The pressure port data from the leading edge and test section are used to generate a pressure distribution, and the angle of attack data band will be defined (Figure 16). The minimum angle of attack (α_{\min}) is the angle at which the pressure side of the airfoil develops a local pressure peak on the glove test surface (forward of $x/c = 0.60$). The maximum angle of attack (α_{\max}) is the angle at which the suction side of the airfoil develops a local pressure peak on the glove test surface. Within the angle of attack range, a desired angle of attack which provides a lift coefficient (C_l) of 0.5 or greater is then recorded for various Mach/Reynolds number combinations. Initially, 0.75 Mach number will be constant while Re_c will vary from 22 million to the glove limits. Wing fuel loading will be noted during these operations in order to understand its effect on C_l . A similar procedure will be followed at 0.72 and 0.66 Mach numbers. The data gathered during the science envelope definition sorties are critical to the subsequent investigations because the NLF and DRE leading edge configurations will not have pressure ports. The desired angle of attack must be matched in order to reproduce the necessary pressure distributions for the remainder of the research program.

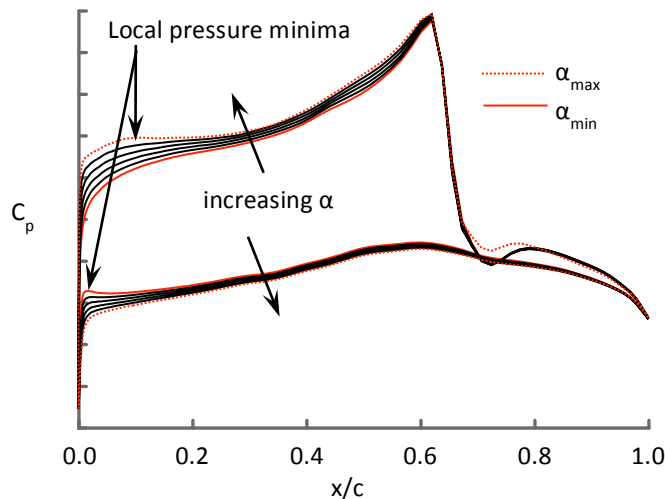


Figure 16. Notional SARGE glove pressure distribution

After the science envelope is defined, Natural Laminar Flow sorties are executed to demonstrate the relationship between Re_c and transition location for polished ($\sim 0.3 \mu\text{m rms}$) and painted leading edges ($\sim 4.0 \mu\text{m rms}$). Data are collected in order to validate stability models and identify the Re_c data band for the subsequent DRE investigation. This block is expected to utilize 2 to 4 sorties and 4 to 8 flight hours. First, at 0.75 Mach number, the Re_c required for a transition location of $x/c = 0.60$ (the aft extent of the test section) is determined. If this is less than 17 million, then 0.72 and 0.66 Mach numbers will be used to investigate the transition location on the test section. Finally, the

relationship between transition location and Re_c with a painted leading edge will be investigated in order to provide a baseline for the subsequent DRE demonstration block.

Finally, the effectiveness of the DREs can be investigated. The data collected in the previous two blocks are critical to properly executing the DRE sorties. The results of the science envelope definition sorties produce the target angle of attack that enables NLF on both the suction and pressure sides of the SARGE glove and gives a minimum C_l of 0.5. The results of the NLF sorties produce a baseline transition location Re_c which is used to demonstrate DRE effectiveness within the science envelope. If the DREs are to delay transition, the NLF transition point must occur no further aft than $x/c = 0.40$ so that a 50% increase in transition location could be detected within the chordwise extent of the SARGE glove ($x/c = 0.60$). Starting with 0.75 Mach number, if the transition location is aft of $x/c = 0.40$ and Re_c is greater than 30 million, only the painted leading edge will be used for the DRE sorties. If the DREs don't delay transition 50% beyond the NLF data at 0.75 Mach number, data will be collected at 0.72 and 0.66 Mach numbers in order to determine the effect of supercritical flow on DRE effectiveness.

Several configurations of DREs will be tested—none of which can be changed in flight. A nominal appliqué DRE height is 10 μm and can be stacked for greater heights. Using these stacks, data will be collected on appliqué DREs with heights from 10 to 50 μm . Circular and rectangular DRE geometries will be investigated. Also, multiple spanwise-periodic DRE intervals will be investigated: control spacing will delay the transition location on the glove test surface, while a critical spacing will excite the most unstable crossflow wave and transition will be *forward* of the NLF transition location. Finally, as previously mentioned, both polished and painted SARGE glove leading edges will be utilized if practicable. As this block is composed of many different configurations, the DRE block will use 32 to 40 sorties and 64 to 80 flight hours.

C. Instrumentation

A research instrumentation suite capable of measuring surface infrared (IR) signatures, static pressures, surface temperatures, boundary layer frequency spectra, and local glove flight conditions has been developed. Additionally, glove gap pressures and wing deflection will be monitored to assure safety of flight and data quality respectively. A long-wavelength infrared camera will be used as the primary boundary layer transition detection tool and will image adiabatic wall recovery temperature and the difference between laminar and turbulent boundary layer heat transfer rates. Two rows of static pressure ports will be used to measure chordwise pressure coefficients and to enable the calculation of the glove lift coefficient. Surface mounted thermocouples will provide wall temperature measurements while uncalibrated hotfilms will provide boundary layer frequency spectrum measurements. An air data boom consisting of a multi-hole probe and high frequency pressure transducers will provide local glove flight conditions. A standard camera combined with calibrated wing markings will be used to determine wing deflection.

1. Infrared (IR) camera

The FLIR SC7750-L long wavelength IR camera has been selected to meet the requirements for the SARGE project. The camera utilizes a mercury-cadmium-telluride detector and has a spectral range of 8.0 μm to 9.4 μm . The manufacturer offers a calibration range of -60°C (-76 °F) to +50°C (+122 °F) and quotes $\pm 1^\circ\text{C}$ accuracy within this range. The IR camera will be the primary boundary layer transition detection tool on the glove's suction side. Under adiabatic wall conditions the camera will measure adiabatic wall recovery temperature and use the difference between these temperatures for laminar and turbulent boundary layers to identify transition. When heat transfer is present, the camera will detect differences in convective cooling rates between laminar and turbulent zones.

The SC7750-L offers many options for lenses, ranging in focal length from 12 mm to 200 mm. The project anticipates using a 12 mm wide-angle lens capable of imaging the entire test section as well as several longer focal length lenses capable of resolving regions of interest. The project is currently evaluating the prospects of using a 200 mm lens to visualize crossflow vortices using the IR camera.

The IR camera will be mounted on the port side of the cabin behind a specially manufactured IR-transparent window. The camera's location is coincident with the G-III's emergency window exit hatch. The hatch window will be modified to allow both IR and standard cameras to image the test surface. An IR image showing a typical perspective of the SARGE glove location is shown in Figure 17.

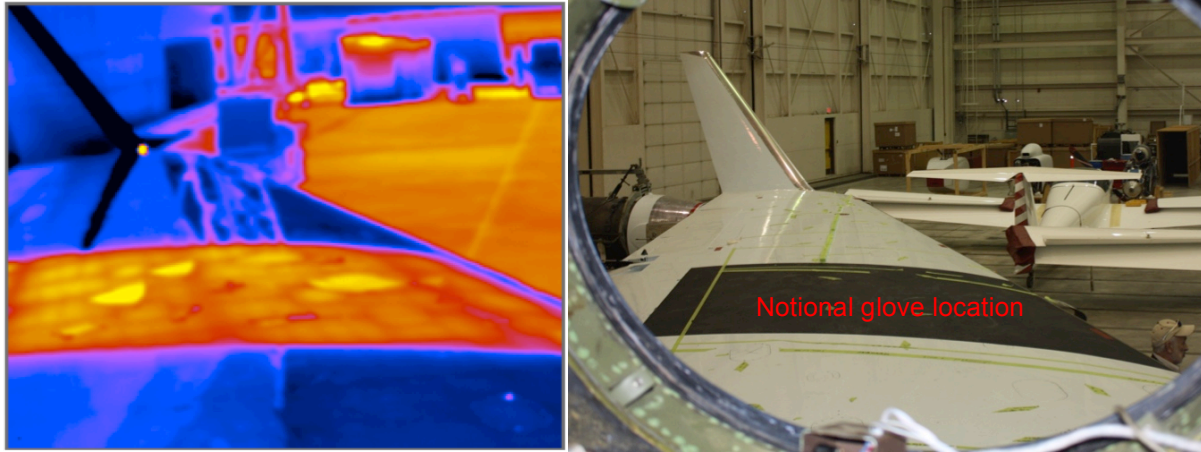


Figure 17. Representative IR camera view through G-III exit window

2. *Glove pressure measurements*

Static pressure measurements will be made using rows of static ports located near the inboard and outboard edges of the glove. The location of the rows has been notionally set at 0.15 m (6.0 in) from either edge of the glove, but will be subject to change following the final glove design optimization. Each row will consist of 29 individual ports of 0.50 mm (0.020 in) diameter for a total of 58 ports on the glove. Both rows will have 23 suction-side and 6 pressure-side ports. These measurements will be used to calculate pressure and lift coefficients during the science envelope definition flights.

3. *Surface-mounted instrumentation*

A surface instrumentation package consisting of uncalibrated hotfilms and thermocouples will be installed on both the pressure and suction sides of the glove. On the pressure side, the surface-mounted instruments will serve as the primary boundary layer transition detection tools. Suction side surface instruments will serve to verify the boundary layer transition results measured with the IR camera. On both the pressure and suction sides care must be taken to place the sensors such that they do not affect downstream measurements.

Uncalibrated hotfilm sensors will be used to measure the boundary layer frequency spectra at various chordwise locations. Eight sensors are to be attached to the suction side of the glove. The current notional layout calls for rows of four sensors along the inboard and outboard edges of the glove. The final locations of these hotfilms will be determined after initial IR thermography data are collected to determine the regions of greatest interest for hotfilm data collection. Five sensors are planned for the pressure side of the glove. These hotfilm sensors are to be installed every ten percent chord beginning at $x/c = 0.20$ and ending at $x/c = 0.60$.

Type-T thermocouples will also be installed on the suction and pressure sides of the glove in order to measure surface temperature. These thermocouples are designed for operation between -60°C (-76°F) and $+175^{\circ}\text{C}$ ($+347^{\circ}\text{F}$). Four thermocouples are anticipated for the suction side. Similar to the hotfilms, the locations of these sensors will be determined after initial IR data have identified regions of interest. Ten thermocouples are planned for the pressure side and will be arranged as inboard and outboard rows of five sensors. Each row is to have thermocouples placed every $x/c = 0.10$ increments, $x/c = 0.20$ to $x/c = 0.60$. A notional suction-side surface instrumentation package is shown in Figure 18; pressure-side instrumentation is similar.

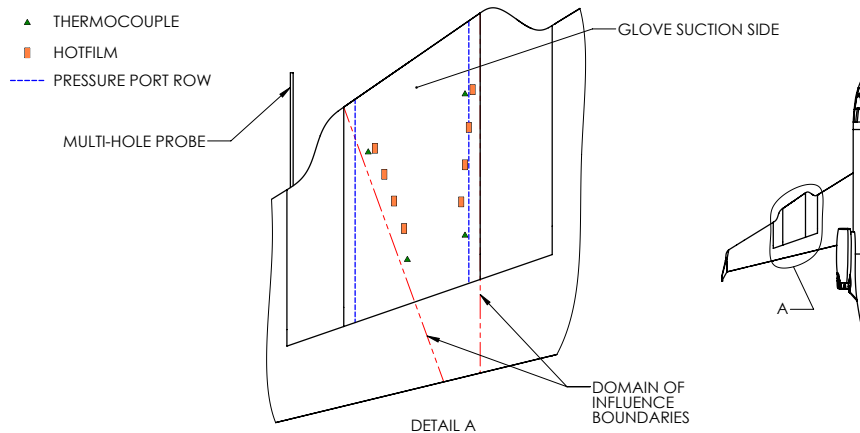


Figure 18. Notional suction-side surface instrumentation

4. Air Data Boom

An air data boom consisting of a multi-hole probe and two high frequency pressure transducers as well as a fuselage-mounted total temperature probe will provide the primary data used by the flight crew to control mission critical aircraft parameters. The multi-hole probe is considered to be a low frequency instrument and will be sampled at 100 Hz. This measurement will be used to establish the glove's mean flow conditions for analysis and model validation. High-frequency transducers will be used to measure disturbance quantities.

The multi-hole probe will directly measure the local static and dynamic pressures. From these data, the angle of attack and effective glove sweep angle (derived from sideslip) can be calculated. Data from the multi-hole probe and the fuselage-mounted total-temperature probe are combined to determine the local glove Mach and Reynolds numbers. Due to the aforementioned tight tolerances on angle of attack, angle of sideslip, Mach number, and Reynolds number, the multi-hole probe must be precise. In order to maintain $AoA_{aircraft}$ and $AoSS_{aircraft}$ tolerance of 0.1° , it is desired to measure both angular measurements with resolutions of at least 0.01° to 0.05° . Mach number must be resolved to 0.005 at worst and Reynolds number must be resolved to no more than 100,000 (when considering the propagation of errors in the constituent measurands). The length and specific location of the boom are currently under analysis. Because the flow streamlines curve outboard upstream of the wing, the boom will likely be located outboard of the glove test section to avoid flow contamination.

Two high frequency pressure transducers will be used to monitor free-stream fluctuations. One will monitor total pressure while the other will monitor static pressure. This will allow the team to collect information about freestream velocity perturbations and acoustic disturbances at the glove. High-speed sampling will be conducted at 150 kHz to capture rapid pressure fluctuations.

5. Standard Camera

A standard camera will also be employed by the team in order to monitor wing deflection. This camera will be located near the IR camera and will take pictures of the wing through different windows of the same specially adapted exit hatch. The surface of the wing will be marked at several locations and an image of the markings will be taken with the wing at a known deflection. This image will then be compared with those taken in flight in order to ascertain both the wing deflection and twist during post-flight data reduction.

VI. Conclusions and further work

Computations of the SCRAT flowfield, including the SARGE wing glove, and the initial design of a laminar flow wing glove have been completed. The next step is to complete the final design, including improved spanwise flow uniformity and better control of TS instabilities. Additional work will include manufacturing tolerance studies, TS sensitivity to temperature deviations, and 3D boundary-layer stability computations using viscous, full-aircraft computations. The design optimization and viscous stability computation efforts will be described in the following sections.

A. Design optimization and refinement

The primary focus of current efforts is to optimize the design to improve the spanwise flow uniformity. Another goal is to minimize the extent of supersonic flow so that the full-aircraft glove C_p more closely approximates the desired C_p of the infinite-span airfoil. This is a collaborative effort between TAMU and DFRC. The effort comprises two parts: 1) finalizing the target C_p distribution and evaluating the boundary-layer stability characteristics of the design and 2) utilizing a design optimization routine to calculate a glove OML that matches the input C_p . The design covered in this paper provides the initial glove shape that starts the optimization routine. Detailed analysis including computations of the linear and nonlinear parabolized stability equations will verify the effectiveness of the design.

B. Viscous stability computations

In previous studies (Wie and Malik 2010, Belisle et. al. 2010) as well as the majority of work discussed above, stability behavior was studied using codes employing direct boundary-layer (DBL) calculations. DBL theory, however, cannot account for the totality of three-dimensional effects (e.g., wing taper and engine effects) expected on the SARGE experiment, due to the assumption of an infinite-swept-wing (e.g., WINGBL2) or the assumption of a conical wing (e.g., Q3BL). DBL calculations are also frequently inaccurate for surfaces with small imperfections, such as two-dimensional waviness, or manufacturing imperfections (Nayfeh et. al. 1987, Wie and Malik 1998). To validate the applicability of these codes to the SARGE geometry and to extend the team's ability to accurately predict stability behavior to situations for which DBL is invalid, the next step will be to employ a full Navier-Stokes solution (e.g., FLUENT) to produce the mean flow required for stability calculations.

Once a suitable solution of the flow field surrounding SARGE is obtained through a Navier-Stokes code, the velocities will be interpolated to a grid-oriented normal to the surface of SARGE. These data will then be used to provide the necessary information to calculate the expected stability behavior. This method has been used successfully by Texas A&M in past experiments (Rhodes et. al. 2008).

Viscous calculations will also be used to define tolerances for manufacturing imperfections. Using a method developed in previous studies (Wie and Malik 1998), the change in N -factor expected by configurations of waviness can be correlated to a single equation for a given geometry and flight condition. A small number of exemplary waviness configurations will be chosen, and from those data, a correlation of the form developed by Wie and Malik will be selected for the SARGE geometry at the most stringent flight condition that is likely to be experienced during the experiment. Doing so will provide an upper bound for the change in stability behavior that would be caused during the SARGE experiment by a given configurations of imperfections. These data will allow the team to set tolerances on the manufacturing imperfections of the SARGE.

Acknowledgments

This work was supported under ViGYAN subrecipient grant C10-00350, ATK grant SP00029509, and AFOSR grant A4760.

This work is a cooperative effort with NASA Dryden Flight Research Center and NASA Langley Research Center. Technical interactions with the NASA Centers are gratefully acknowledged. A companion paper (Malik et al., 2011) describes additional results and computations on the design.

References

- ¹ Arnal D, Casalis G. 2000 Laminar-turbulent prediction in three-dimensional flows. *Progress in Aerospace Sciences*. 36(2):173–91
- ² Arnal D, Vermeersch O. 2011 Compressibility effects on laminar–turbulent boundary layer transition. *International Journal of Engineering Systems Modeling and Simulation* 3(1): 26–35.
- ³ Belisle MJ, Neale TP, Reed HL, Saric WS. 2009 Design of a Swept-Wing Laminar Flow Control Flight Experiment for Transonic Aircraft. *AIAA-2010-4381*
- ⁴ Saric WS, Carpenter AL, Reed HL. 2011 Passive control of transition in three-dimensional boundary layers, with emphasis on discrete roughness elements. *Phil. Trans. R. Soc. A* 369:1352–64
- ⁵ Carpenter AL, Saric WS, Reed HL. 2010 Roughness Receptivity in Swept-Wing Boundary Layers—Experiments. *Int'l J. Eng. Sys. Modeling and Simulation*, 2(1):128-38
- ⁶ Chang C-L. 2003 The Langley stability and transition analysis code (LASTRAC): LST, linear & nonlinear PSE for 2-D, axisymmetric, and infinite swept wing boundary layers. *AIAA-2003-0974*

- ⁷ Chang C-L, Choudhari M. 2005 Boundary-layer receptivity and integrated transition prediction. *AIAA-2005-0526*
- ⁸ Drela M. 1989 Xfoil—an analysis and design system for low Reynolds number airfoils. *Low Reynolds Number Aerodynamics* pp. 1–12
- ⁹ Malik M. 1997 Boundary-layer transition prediction toolkit. *AIAA-1997-1904*.
- ¹⁰ Malik M, Liao W, Lee-Rausch E, Li F, Choudhari M, Chang C-L. 2011 Computational Analysis of the G-III Laminar Flow Glove. *AIAA-2011-3525*.
- ¹¹ Menter FR. 1993 Zonal Two Equation k- ϵ , Turbulence Models for Aerodynamic Flows. *AIAA-1993-2906*
- ¹² Nayfeh AH, Ragab SA, Al-Maaitah AA. 1988 Effect of Bulges on the Stability of Boundary-Layers. *Physics of Fluids* 31(4): 796–806
- ¹³ Pruett CD. 1994 A spectrally accurate boundary-layer code for infinite swept wings. NASA Contractor Report 195014
- ¹⁴ Pfenninger W. 1997 Laminar flow control—Laminarization. *AGARD Report No. 654*
- ¹⁵ Poll DIA. 1985 Some observations of the transition process on the windward face of a long yawed cylinder. *J. Fluid Mech.* 150:329-56
- ¹⁶ Rizzetta D, Visbal M, Reed HL, Saric WS. 2010 Direct numerical simulation of discrete roughness on a swept wing leading edge. *AIAA J.* 48(11):2660–73
- ¹⁷ Rhodes RG, Reed HL, Saric WS, Carpenter AL. 2010 Roughness Receptivity in Swept-Wing Boundary Layers—Computations. *Int'l J. Eng. Sys. Modeling and Simulation.* 2(1):139–48
- ¹⁸ Saric WS, Carrillo RB, Reibert MS. 1998 Leading-edge roughness as a transition control mechanism. *AIAA-1998-0781*
- ¹⁹ Saric WS, Reed HL, Banks DW. 2004 Flight testing of laminar flow control in high-speed boundary layers. *NATO-RTO-MP-AVT-111*, Prague, Oct.
- ²⁰ Vassberg JC, Tinoco EN, Mani M, Rider B, Zickuhr T, David WL, Brodersen OP, Eisfeld B, Crippa S, Wahls RA, Morrison JH, Mavriplis DJ, Murayama M. 2010 Summary of the Fourth AIAA CFD Drag Prediction Workshop. *AIAA-2010-4547*
- ²¹ Wie Y-S, Malik MR. 1998 Effect of Surface Waviness on Boundary-Layer Transition in Two-Dimensional Flow. *Computers and Fluids* 27(2): 157–181
- ²² MIL-F-8785C. 1980. Flying Qualities of Piloted Airplanes.